J. Fluid Mech. (2008), *vol.* 598, *pp.* 267–292. © 2008 Cambridge University Press
doi:10.1017/S0022112007000043 Printed in the United Kingdom

The analysis of self-diffusion and migration of rough spheres in nonlinear shear flow using a traction-corrected boundary element method

MARC S. INGBER[1], SHIHAI FENG[2], ALAN L. GRAHAM[2] AND HOWARD BRENNER[3]

[1]Department of Mechanical Engineering, University of New Mexico, Albuquerque, NM 87131, USA
[2]Institutes Division, Los Alamos National Laboratory, Los Alamos, NM 87545, USA
[3]Department of Chemical Engineering, Massachusetts Institute of Technology, Cambridge, MA 02139, USA

(Received 8 December 2006 and in revised form 1 November 2007)

The phenomena of self-diffusion and migration of rough spheres in nonlinear shear flows are investigated using a new traction-corrected boundary element method (TC-BEM) in which the near-field asymptotics for the traction solution in the interstitial region between two nearly touching spheres is seamlessly coupled with a traditional direct boundary element method. The TC-BEM is extremely accurate in predicting particle trajectories, and hence can be used to calculate both the particle self-diffusivity and a newly defined migration diffusivity for dilute suspensions. The migration diffusivity is a function of a nonlinearity parameter characterizing the shear flow and arises from the net displacement of the centre of gravity of particle pairs. This net displacement of the centre of gravity of particle pairs does not occur for smooth particles, nor for rough particles in a linear shear flow. An explanation is provided for why two-particle interactions of rough spheres in a nonlinear shear flow result in particle migration.

1. Introduction

Shear-induced self-diffusion and particle migration in suspension flows are important in a variety of scientific and engineering applications such as the transport of sediments, chromatography, composite materials processing, secondary oil recovery techniques, and sequestration processes in porous media, to name a few. Significant research effort has been undertaken in the past several decades to understand how these phenomena influence the modelling of suspension flows under conditions such that hydrodynamic forces are dominant.

Shear-induced particle diffusion was studied experimentally by Eckstein, Bailey & Shapiro (1977), who monitored the motion of a tagged particle within a suspension being sheared in a Couette device. For moderate concentration of particles, they found the self-diffusivity, D, of the random walk across the streamlines was proportional to $\dot{\gamma}a^2$, where $\dot{\gamma}$ is the local shear rate and a is the radius of the particle, with proportionality coefficient of order 0.025. At low-volume fractions ($\phi < 0.2$), they found that the diffusivity was approximately linear in the concentration of the suspension. Leighton & Acrivos (1987*a*, *b*) examined the phenomenon in more detail by reporting experimental values for the lateral diffusion coefficient within the plane

https://doi.org/10.1017/S0022112007000043 Published online by Cambridge University Press

of shear given by $D \approx 0.5\phi^2\dot{\gamma}a^2$ for $0.05 < \phi < 0.4$. The numerical simulations by Bossis & Brady (1987) and Chang & Powell (1994) for a suspension confined to a monolayer agreed qualitatively with the results of Leighton & Acrivos (1987*a*, *b*) for the self-diffusivity coefficient. da Cunha & Hinch (1996) studied the self-diffusivity of rough spheres at low concentrations in a linear shear flow analytically by using the exact two-sphere solutions of Batchelor & Green (1972), the mobility functions provided by Kim & Karrila (1991), and by controlling the motion parallel and normal to the line of centres of the spheres. For roughnesses $0 < \epsilon/a < 0.08$, da Cunha & Hinch determined the self-diffusivity in the plane of shear to be in the range $0 < D/(\phi a^2\dot{\gamma}) < 0.03$. They determined further that the out-of-plane self-diffusivity should be an order of magnitude less than the in-plane self-diffusivity. Brady & Morris (1997) determined that the asymmetry of the pair-distribution function and boundary layer structure yielded a shear-induced self-diffusivity of $O(\dot{\gamma}a^2\phi)$ as the Péclet number $Pe \to \infty$. Their results were qualitatively similar to those of da Cunha & Hinch.

Shear-induced particle migration has been studied experimentally by several groups (Leighton & Acrivos 1987*b*; Phillips *et al.* 1992; Tetlow *et al.* 1998; Hsiao *et al.* 2003). There is now substantial evidence that particle migration occurs in sheared suspensions due to gradients in the shear rate, gradients in the particle concentration, and gradients in the effective suspension viscosity. Leighton & Acrivos (1987*b*) attribute one of the causes of particle migration to the fact that, in the presence of concentration and shear rate gradients, a test sphere will experience more interactions on one of its sides than on the other, resulting in drift of the particle from regions of higher particle interactions to regions of lower particle interactions. Phillips *et al.* (1992) used the scaling arguments of Leighton and Acrivos to develop the diffusive flux model for suspension flows that accounted for shear-induced particle migration. This model was refined by Fang *et al.* (2002) to account for the different rates of migration in the shear plane as opposed to the vorticity plane. In another rheological model originally proposed by Nott & Brady (1994), designated as the suspension balance model, the stress in the particle phase is described by a constitutive equation, and particle transport is driven by gradients in this stress. The suspension balance model was refined by Morris & Boulay (1999) and Fang *et al.* (2002) to account for non-isotropic migration rates. Additional rheological models based on mixture theory have been proposed by Pozarnik & Skerget (2003) and Buyevich (1995). However, all of the models proposed to date predict that particle migration should scale with the radius of the particle squared. Unfortunately, the experimental data (Abbott *et al.* 1991; Tetlow *et al.* 1998; Hsiao *et al.* 2003) does not support this scaling, and hence, none of the models can be used to reliably predict transient concentration profiles.

Mesoscopic simulations can provide valuable information about particle interactions of suspended particles in nonlinear shear flow, which can potentially provide insight into some of the problems of the current rheological models discussed above. However, for suspension flows, particles tend to chain and agglomerate (Graham & Bird 1984; Mammoli & Ingber 2000), resulting in complex multiply connected computational domains and extremely stiff differential systems. In fact, as solid surfaces approach in Stokes flow, the analytical solutions become nearly singular (Brenner 1961; Cooley & O'Neill 1969; Jeffrey & Onishi 1984). A manifestation of this for suspension flows is that, as the gap between adjacent particles becomes small, the interstitial tractions, as calculated by most mesoscopic numerical

https://doi.org/10.1017/S0022112007000043 Published online by Cambridge University Press

simulation methods, are typically underpredicted, resulting in the relative velocities between particles being overpredicted (Hampton, Mammoli & Ingber 2003; Mammoli 2005; Sangani & Mo 1994; Dance & Maxey 2003).

The numerical problems associated with solid surfaces in close proximity in Stokes flow has been recognized for some time. Ascoli, Dandy & Leal (1989) considered the problem of a sphere interacting with a planar wall using a modified boundary element method (BEM) based on a wall Green's function. They were able to determine accurate results up to dimensionless gaps between the sphere and the wall of 0.05. For smaller gaps, the results diverged from the analytic results. Chan, Beris & Advani (1992) developed a second-order BEM to analyse flow about particles in close proximity. They determined that their BEM solutions diverged from analytical solutions for separations below approximately 1% of a particle radius. However, with adaptive subdomain integration, they were able to improve their results. Ingber, Subia & Mondy (2000) used the so-called Telles transformation (Telles & Oliveira 1994) to reduce quadrature errors associated with the nearly singular integrals, caused by surfaces being in close proximity, to improve the solution accuracy of following particle trajectories in viscous flows.

As discussed above, particles suspended in shear flows tend to agglomerate and chain resulting in extremely small inter-particle separations. In these situations, the over-prediction of the relative particle velocities can result in non-physical particle overlap. Further, the numerical problems are so severe that even adaptive mesh refinement does not provide an adequate convergence rate to overcome these problems (Mammoli 2005). Thus, a number of researchers have developed methods of incorporating lubrication approximations based on two-body interactions into their numerical formulations.

Stokesian Dynamics (SD) is based on decomposing hydrodynamic interactions between particles into far-field mobility interactions and near-field pairwise additive 'lubrication' interactions (Nott & Brady 1994). SD simulations have been used in a variety of applications including the effective viscosity of monomodal suspensions (Brady & Bossis 1985) and bimodal suspensions (Chang & Powell 1994), the pair-distribution function of sheared suspensions (Sierou & Brady 2002), sedimentation characteristics (Sierou & Brady 2001), and shear-induced particle diffusivities (Marchioro & Acrivos 2001).

Dance & Maxey (2003) incorporated near-field lubrication effects into their force-coupling method (FCM) in order to more accurately follow the trajectories of particles in close proximity. Although the lubrication correction improved their results, they still found it necessary to employ an additional repulsive force to prevent occasional particle overlap.

Sangani & Mo (1994) incorporated close-field lubrication forces between pairs of particles in multiparticle Stokes flow. They used the method of multipole expansion based on a periodic Green's function in which the source density was split into a contribution in the multipole expansion and a component due to the lubrication forces between particle pairs. They used their method to determine the drag on an array of cylinders. Sangani & Mo (1996) improved their method by reducing the operation count and extended their analysis to consider the effective viscosity and sedimentation characteristics of suspended spheres.

Nasseri *et al.* (2000) incorporated short-range lubrication effects into the completed double-layer boundary element method (CDL-BEM) to determine the effective viscosity of suspensions from the dilute to concentrated regimes. They proposed

https://doi.org/10.1017/S0022112007000043 Published online by Cambridge University Press

that, whenever the gap between particles was less than a critical value, the particles would be excluded from the CDL-BEM formulation and their effects would be modelled using the lubrication equations. Their results for the effective suspension viscosity improved dramatically by including the lubrication effects.

Although the methods discussed above, incorporating the near-field lubrication effects into numerical simulations, generally gave good approximation of the gross features of suspension flows such as the effective viscosity, hindered settling correlation, pair-distribution function, and composite drag, they were not benchmarked or compared to experiment to determine whether they could accurately follow particle trajectories. It has been shown that very small errors in a particle velocity can result in large changes in the particle trajectory (Jayaweera, Mason & Slack 1964; Jánosi *et al.* 1997; Ingber *et al.* 2006).

Mammoli (2005) developed the lubrication-corrected completed double-layer boundary integral equation (LC/CDL-BIE) method in order to perform detailed studies of particle trajectories in Stokes flow. His method was based on an approach developed by Zinchenko (1998) to study the effective conductivity of granular materials. In this approach, when a collocation point on a given particle was close to an adjacent particle, the particle containing the collocation point was shrunk anywhere from 2 % to 5 %. In order to correct for the shrinkage, a combination of analytic values for the resultant forces and moments on the particles were added to the range completer in the CDL-BIE. This approach resulted in excellent near- and far-field approximations. However, there was a small range of particle separations on the order of 1 % of the characteristic particle diameter in which the intermediate field approximation was relatively poor. Although for bulk quantities such as an effective viscosity of a suspension, the LC/CDL-BIE yielded excellent results (Mammoli 2002), the method could not resolve individual particle trajectories accurately enough to calculate quantities such as particle self-diffusivity since the two-particle interactions would very often go through the region of maximum pain on the order of 1 % of the characteristic particle diameter where the intermediate field was not well resolved.

In the current research, a new method is developed to incorporate the near-field effects into the boundary element method. Rather than working with lubrication forces, as done previously (Bossis & Brady 1984; Dance & Maxey 2003; Sangani & Mo 1994; Nasseri *et al.* 2000; Mammoli 2005), asymptotic solutions have been derived for the traction field in the interstitial regions between particles. The calculation of the traction unknowns, for a single boundary element centred around the point of nearest contact, is based solely on the relative motion of the two particles in terms of the asymptotic traction solutions rather than on boundary element collocation within that element. In this way, the system remains fully coupled, incorporating the boundary element representation for all other elements along with the near-field asymptotics. This new traction-corrected boundary element method (TC-BEM) is capable of accurately predicting particle trajectories, and hence can be effectively used as a mesoscopic tool to study particle self-diffusion and migration in nonlinear shear fields.

The organization of this paper is as follows. In § 2, the formulation for the near-field asymptotic traction solution for solid spheres suspended in a viscous fluid is presented. In § 3, the TC-BEM formulation is presented. In § 4, the TC-BEM is benchmarked by comparison with the analytic solution for the interaction of two spheres in a linear shear field. Although this problem has been studied previously (da Cunha & Hinch 1996), some new results are presented characterizing the effects of surface roughness on the resulting irreversibility in the particle trajectories. In § 5, the results of an

https://doi.org/10.1017/S0022112007000043 Published online by Cambridge University Press

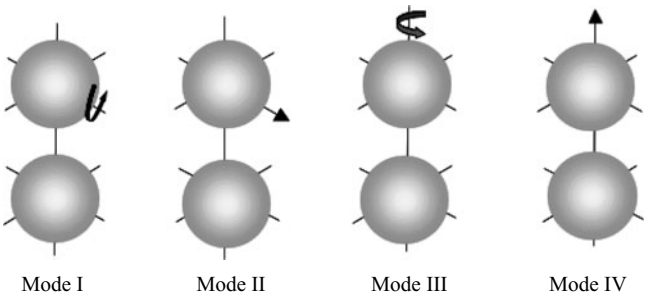


FIGURE 1. The four modes of relative motion of two spheres suspended in a viscous shear flow.

extensive study of self-diffusion and particle migration of rough spheres in nonlinear shear flows is presented. Finally, in § 6, some conclusions are drawn.

2. Near-field asymptotic traction solution for solid spheres suspended in a viscous fluid

The relative motion of two spheres suspended in a viscous shear flow can be decoupled into 4 basic modes of motion, as shown in figure 1. These motions are given by one sphere rotating relative to the other sphere about a line perpendicular to their line of centres (mode I), one sphere translating relatively to the other sphere along a line perpendicular to their line of centres (mode II), one sphere rotating relative to the other sphere about their line of centres (mode III), and one sphere translating relative to the other sphere along their line of centres (mode IV). Asymptotic solutions for the velocity and pressure field for all four modes in the interstitial region between two nearly touching spheres can be derived using well-known lubrication approximations. Despite the fact that the governing asymptotic equations for all four modes of motion have been previously derived by Cox & Brenner (1967), Corless & Jeffrey (1988), and O'Neill & Majumdar (1970*b*, *a*), none of these researchers provided the complete solutions to the equations since their primary interest was the resultant force and moment exerted by one sphere on the other.

The governing equations for steady-state, creeping fluid flow are given by

$$\nabla \cdot \boldsymbol{u}' = 0, \tag{2.1}$$

$$\nabla \cdot \boldsymbol{\sigma}' = 0. \tag{2.2}$$

The total stress field $\boldsymbol{\sigma}'$ is given by

$$\boldsymbol{\sigma}' = -p'\boldsymbol{I} + \mu(\nabla \boldsymbol{u}' + \nabla \boldsymbol{u}'^{\mathrm{T}}), \tag{2.3}$$

where p' is the hydrostatic pressure, $\boldsymbol{I}$ is the unit tensor, μ is the constant viscosity of the suspending fluid, and the superscript T denotes the transpose operator. The boundary traction field is defined by

$$\boldsymbol{t}' = \boldsymbol{n} \cdot \boldsymbol{\sigma}' \tag{2.4}$$

where $\boldsymbol{n}$ is the unit normal vector pointing outward from the fluid field.

In the following, sphere A is moving while sphere B is at rest and sphere A is positioned directly above sphere B. A cylindrical coordinate system is chosen (r', θ, z') whose origin lies on the surface of sphere B at the closest point to sphere A. The minimum separation distance between the closest points of sphere A and B is δ

https://doi.org/10.1017/S0022112007000043 Published online by Cambridge University Press

where, for the asymptotic analysis considered herein, $\delta \ll a$. The velocity components are given by (u', v', w').

The cylindrical coordinates r' and z' are first non-dimensionalized and then stretched using the equations

$$r = \frac{r'}{a}, \qquad z = \frac{z'}{a}, \tag{2.5}$$

$$r^* = \sqrt{\frac{a}{\delta}}r, \qquad z^* = \frac{az}{\delta}. \tag{2.6}$$

The equations of surfaces of A and B are now given in terms of the stretched coordinates by

$$z^* = \frac{\delta (r^*)^4}{8a} + \frac{(r^*)^2}{2} + 1 + O\left(\left(\frac{\delta}{a}\right)^2\right) \quad \text{on sphere A,} \tag{2.7}$$

$$z^* = -\frac{\delta (r^*)^4}{8a} - \frac{(r^*)^2}{2} - O\left(\left(\frac{\delta}{a}\right)^2\right) \quad \text{on sphere B.} \tag{2.8}$$

For mode I motion, the non-dimensional pressure and velocity components are given by

$$p(r,z) = \frac{p'}{\mu \Omega^I \cos(\theta)}, \quad u(r,z) = \frac{u'}{a\Omega^I \cos(\theta)}, \quad v(r,z) = \frac{v'}{a\Omega^I \sin(\theta)}, \quad w(r,z) = \frac{w'}{a\Omega^I \cos(\theta)} \tag{2.9}$$

where Ω^I is the rotation rate of sphere A about an axis perpendicular to the line of centres. The non-dimensional scaled expansions of the flow field in the inner gap region are given by

$$p = \left(\frac{\delta}{a}\right)^{-3/2} p_1 + \left(\frac{\delta}{a}\right)^{-1/2} p_2 + O\left(\left(\frac{\delta}{a}\right)^{1/2}\right), \tag{2.10}$$

$$u = u_1 + \frac{\delta}{a}u_2 + O\left(\left(\frac{\delta}{a}\right)^2\right), \tag{2.11}$$

$$v = v_1 + \frac{\delta}{a}v_2 + O\left(\left(\frac{\delta}{a}\right)^2\right), \tag{2.12}$$

$$w = \left(\frac{\delta}{a}\right)^{1/2} w_1 + \left(\frac{\delta}{a}\right)^{3/2} w_2 + O\left(\left(\frac{\delta}{a}\right)^{5/2}\right) \tag{2.13}$$

(O'Neill & Majumdar 1970*b*; Jeffrey & Onishi 1984; Corless & Jeffrey 1988).

The non-dimensional velocity components and pressure for mode II motion are the same as for mode I motion except that $a\Omega^I$ is replaced by U in (2.9), where U is the translational velocity of sphere A. Further, the non-dimensional scaled expansion of the velocity components and pressure are identical to mode I motion.

For mode III motion, the pressure field is identically zero and the only non-zero component of velocity is in the v'-direction. The non-dimensional velocity component is given by

$$v(r,z) = \frac{v'}{a\Omega^{III}}, \tag{2.14}$$

https://doi.org/10.1017/S0022112007000043 Published online by Cambridge University Press

where, in this case, Ω^{III} is the rotation rate of sphere A about the line of centres of the two spheres. The scaled expansion of the velocity component in the inner gap region is given by

$$v = \left(\frac{\delta}{a}\right)^{1/2} v_1 + O\left(\frac{\delta}{a}\right)^{3/2} \tag{2.15}$$

(Jeffrey & Onishi 1984).

For mode IV motion, the non-dimensional pressure and (non-zero) velocity components are given by

$$p(r, z) = \frac{ap'}{\mu W}, u(r, z) = \frac{u'}{W}, w(r, z) = \frac{w'}{W}, \tag{2.16}$$

where W is the separation velocity of sphere A along the line of centres of the two spheres. Following Cox & Brenner (1967), the scaled expansions for p, u, and w are given by

$$p = p_1 + \frac{\delta}{a} p_2 + O\left(\left(\frac{\delta}{a}\right)^2\right), \tag{2.17}$$

$$u = u_1 + \left(\frac{\delta}{a}\right)^{1/2} u_2 + O\left(\left(\frac{\delta}{a}\right)^{3/2}\right), \tag{2.18}$$

$$w = w_1 + \frac{\delta}{a} w_2 + O\left(\left(\frac{\delta}{a}\right)^2\right). \tag{2.19}$$

The first- and second-order governing equations for all four modes of motion can be found in the original references given above (Cox & Brenner 1967; O'Neill & Majumdar 1970*b*; Jeffrey & Onishi 1984; Corless & Jeffrey 1988). However, as discussed above, none of these authors provided the complete solutions for these equations. The asymptotic pressure and velocity solutions up to the orders indicated by (2.10)–(2.13) for mode I and II motion, (2.15) for mode III motion, and (2.17)–(2.19) for mode IV motion are given in the appendices. The stress tensor can then be formed using the well-known constitutive law for Newtonian fluids from the pressure and velocity gradient fields. Finally, the asymptotic traction solution can be determined by contracting the stress tensor with the unit normal vector. The asymptotic traction solutions are not presented in the appendices because of their length.

3. Traction-corrected boundary element formulation

In this section, the traditional direct boundary element formulation for particles suspended in a viscous shear flow is first presented followed by the coupling technique to introduce the near-field asymptotic traction solution in the interstitial region between two nearly touching spheres. The physical system considered comprises rigid spheres suspended in an incompressible, exterior flow of a Newtonian fluid at zero Reynolds number.

The governing continuity and momentum equations, (2.1) and (2.2), can be recast into integral form by considering a weighted residual reformulation of the governing equations with weighting functions given by fundamental solutions of the Stokes equations (Ladyzhenskaya 1969; Youngren & Acrivos 1973; Ingber 1989). The fundamental solution for the velocity field and the associated fundamental solution

https://doi.org/10.1017/S0022112007000043 Published online by Cambridge University Press

for the stress field are given by

$$u^*_{ij}(\xi, x) = \frac{1}{8\pi r}(\delta_{ij} + r_{,i}r_{,j}), \tag{3.1}$$

$$q^*_{ijk}(\xi, x) = \frac{-3}{4\pi}\frac{r_{,i}r_{,j}r_{,k}}{r^2}, \tag{3.2}$$

where r is the distance between ξ and x, δ_{ij} is the Kronecker delta function and the comma denotes differentiation with respect to the appropriate Cartesian coordinate. The resulting boundary integral equation (BIE) is given by (Kim & Karrila 1991)

$$c_{ij}(\xi)\, u_j(\xi) + \int_\Gamma q^*_{ijk}(\xi, x)\, u_k(x)\, n_j(x)\, \mathrm{d}\Gamma = -\int_\Gamma u^*_{ij}(\xi, x)\, t_j(x)\, \mathrm{d}\Gamma, \tag{3.3}$$

where t_k represents the components of the traction along the surface Γ and n_j represents the components of the unit outward-normal vector to the boundary Γ. The coefficient tensor c_{ij} can be determined from the local geometry at the field point or by integrating q^*_{ijk} over Γ. However, for the spherical geometries considered in this paper, $c_{ij} = \delta_{ij}/2$.

The BIE (3.3) is discretized by subdividing the boundary of the domain Γ into superparametric boundary elements in which the geometry is given piecewise quadratic approximation and the traction and velocity components are given piecewise constant approximation. By collocating the BIE at the centre of each element, the following linear equations are generated:

$$[H_{ij}]\{\tilde{u}_j\} = [G_{ij}]\{\tilde{t}_j\}, \tag{3.4}$$

where $\tilde{u}_j$ and $\tilde{t}_j$ represent the values of the components of velocity and stress respectively at the boundary element nodes.

In the current BEM formulation, neither the components of velocity nor traction are known on the surface of the suspended particles. For rigid particles, the velocity components on the particle surface can be related to the six components of linear and angular velocity at the centroids of the particles through a kinematic tensor transformation. That is,

$$\{\tilde{u}_j\} = [K_{jl}]\{U_l\}, \tag{3.5}$$

where U_l represents the velocities (linear and angular) at the centroids of the particles.

The algebraic system of equations is closed in the quasi-static analysis by enforcing equilibrium equations in which the resultant forces and moments on the particles generated by the surface tractions and body forces are set to zero. That is,

$$\int_{\Gamma_i} \boldsymbol{n}\cdot\boldsymbol{\sigma}\, \mathrm{d}\Gamma + \boldsymbol{b}^i = 0, \tag{3.6}$$

$$\int_{\Gamma_i} (q - q^i) \times (\boldsymbol{n}\cdot\boldsymbol{\sigma})\, \mathrm{d}\Gamma = 0, \tag{3.7}$$

where $\boldsymbol{b}^i$ is the body force acting on the ith particle, and q^i is the location of the centroid of the ith particle. These equations can be represented symbolically in matrix form in terms of the surface tractions as follows:

$$[M_{ij}]\{\tilde{t}_j\} = \{\tilde{b}_i\}. \tag{3.8}$$

https://doi.org/10.1017/S0022112007000043 Published online by Cambridge University Press

The governing linear system is then obtained by combining (3.4), (3.5) and (3.8), which is written as

$$\begin{bmatrix} [G_{ij}] & -[H_{ij}][K_{jl}] \\ [M_{ij}] & 0 \end{bmatrix} \begin{Bmatrix} \{\tilde{t}_j\} \\ \{U_l\} \end{Bmatrix} = \begin{Bmatrix} 0 \\ \{\tilde{b}_i\} \end{Bmatrix}. \tag{3.9}$$

It has been shown previously (Hampton *et al.* 2003; Mammoli 2005) that the convergence characteristics of most numerical methods, including the current boundary element formulation for the analysis of rigid particles suspended in an incompressible flow field, are inadequate as the separation between particles becomes small. Typically, the results of these methods overpredict the relative velocity of the particles and underpredict the interstitial tractions. The convergence and accuracy of the BEM formulation can be vastly improved by incorporating the near-field asymptotic traction solution.

The current TC-BEM is based on a fixed mesh (discretization) for each particle. In particular, a mesh containing 294 boundary elements per sphere is used in the current research, although other meshes could also be used. For any given relative position of the particles, the meshes are rotated so that the boundary element initially centred on the south pole of one sphere is exactly aligned with the boundary element initially centred on the north pole of the second sphere. With the rotated mesh, the linear system of boundary element, kinematic, and equilibrium equations, (3.9), is then generated. Next, the 6 equations of the linear system associated with collocation at the two nodes (one per particle) centred within the two elements in the interstitial region between spheres are replaced using the asymptotic traction solution as described below.

First the average tractions over an interstitial element are tabulated in the TC-BEM computer code for three of the four modes of relative motion discussed in the previous section, namely, mode I, mode II, and mode IV at selected separations, δ/a, between the particles, under the presumption that the linear speed and absolute value of the angular velocity for each particle is unity. Mode III motion need not be considered, since the net contribution of this mode to the overall force and moment exerted on the element is zero. The table has a maximum separation of $\delta/a = 0.2$ and a minimum separation of $\delta/a = 0.00002$ where δ is the minimum surface-to-surface separation between the two spheres. For relative positions of the particles with $\delta/a > 0.2$, no traction correction is used. For $\delta/a < 0.00002$, the simulation is stopped, although smaller separations could be considered by expanding the table. For values of δ/a not in the table, a cubic spline interpolation is used to determine the appropriate traction.

The values of the traction for the 3 modes of relative motion determined from the tabulated data are given by f_1, f_2 and f_4. Again, since f_2 and f_4 are calculated presuming an appropriate relative approach velocity of unity and f_1 is calculated based on a relative rotational velocity of unity, these quantities can be thought of as forces per unit approach velocity. Further, since the traction scales directly with the relative velocities of the particles, the average normal and two tangential traction components, τ_n, τ_{t1}, and τ_{t2}, respectively, for the interstitial elements are given by

$$\begin{Bmatrix} \tau_n \\ \tau_{t1} \\ \tau_{t2} \end{Bmatrix} = \begin{bmatrix} f_4/2 & 0 & 0 & 0 & 0 & 0 \\ 0 & f_2/2 & 0 & 0 & -f_1/2 & 0 \\ 0 & 0 & f_2/2 & 0 & 0 & -f_1/2 \end{bmatrix} \begin{Bmatrix} du_n \\ du_{t1} \\ du_{t2} \\ d\omega_n \\ d\omega_{t1} \\ d\omega_{t2} \end{Bmatrix}, \tag{3.10}$$

https://doi.org/10.1017/S0022112007000043 Published online by Cambridge University Press

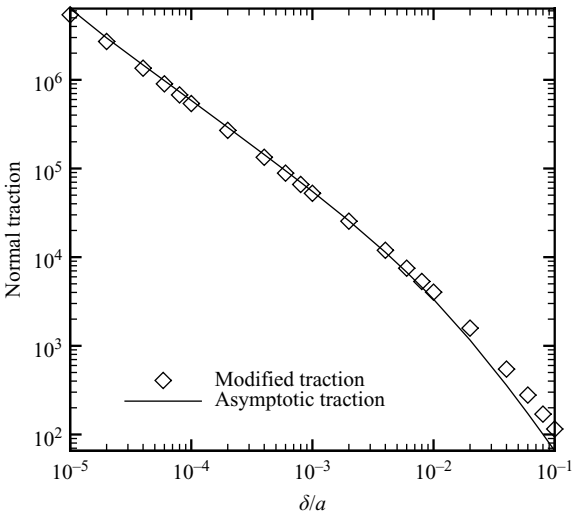


FIGURE 2. Asymptotic and modified tractions for mode IV motion as a function of particle separation, δ/a.

where du_n, du_{t1}, and du_{t2} represent the difference in the appropriate component of velocity between the two spheres and $d\omega_n$, $d\omega_{t1}$, and $d\omega_{t2}$ represent the corresponding differences in the angular velocity components of the two spheres. Since the unknowns in (3.9) include the velocities and tractions in Cartesian coordinates, transformation matrices are applied to (3.10) so that the surface tractions in Cartesian coordinates are related to the velocity differences in Cartesian coordinates.

The approach described above was refined slightly by performing simulations of mode I, mode II, and mode IV motions separately. For example, for mode IV motion, the particles were aligned vertically and a force of known magnitude was applied to each particle so that the analytic solution gave an approach velocity of 1.0 for each particle. Generally, with the traction correction provided by the asymptotic solutions, the TC-BEM provided particle velocities that were slightly different from the analytical solution of 1.0. This discrepancy is mainly caused by the fact that the traction used in the interstitial region is an area-averaged traction as opposed to the exact distribution over the element. To improve the accuracy of the method, the tractions were adjusted slightly so that the analytical velocity could be recovered for all three modes of motion. As an example, the asymptotic traction solution as a function of particle separation, δ/a, is shown in figure 2. Also shown in the figure are the modified tractions, $f4$, that were actually placed in the table to be used in (3.10).

The TC-BEM formulation corresponds to the grand resistance formulation in that the particle velocities are solely a function of position. The particles are repositioned in time using a third-order variable-time-step Runge–Kutta method in which the time step is adjusted based on the local truncation error.

A roughness model has been added to the TC-BEM which restricts the normal motion of the particles if the separation between particles δ becomes less than a specified particle roughness ϵ. This model is essentially equivalent to the non-locked model of da Cunha & Hinch (1996).

https://doi.org/10.1017/S0022112007000043 Published online by Cambridge University Press

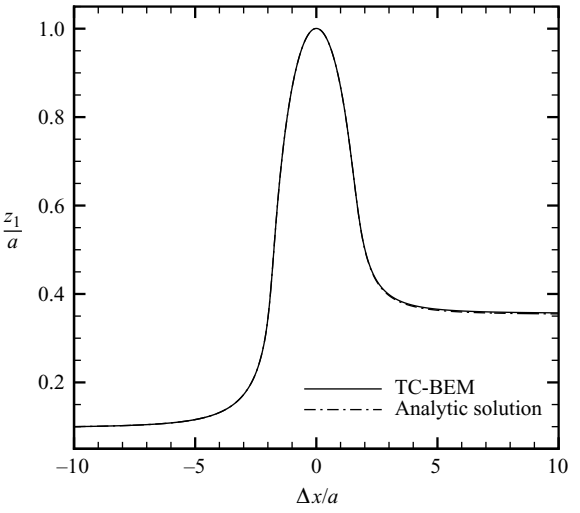


FIGURE 3. Particle trajectories in the shear plane for the upper sphere for the case $\Delta z_{-\infty} = 0.2$ and $\epsilon/a = 1.0 \times 10^{-3}$. Δx is the horizontal separation of the spheres given by $x_1 - x_2$.

4. Numerical benchmarking of the TC-BEM

The numerical benchmarking of the TC-BEM is provided by a series of problems consisting of two particles in a linear shear flow whose centres lie in the same shear plane. In the following section, these simulations will be extended to cases in which the particles do not lie in the same shear plane, and to nonlinear shear flows. The following definitions will be useful in characterizing these problems. The coordinates of the two particles are given by (x_1, y_1, z_1) and (x_2, y_2, z_2). The initial centre-to-centre separations of the spheres in the three coordinate directions are given by $\Delta x_{-\infty}$, $\Delta y_{-\infty}$, and $\Delta z_{-\infty}$. For all simulations the shear plane is the x–z plane, the far-field velocity is in the x-direction, and the initial separation is given by $\Delta x_{-\infty}/a = -10$. The simulations are stopped when $x_2 - x_1 = 10a$, which then sets the downstream separations denoted by Δx_{∞}, Δy_{∞}, and Δz_{∞}. The particle trajectories are typically drawn with respect to the transient separation $\Delta x = x_1 - x_2$.

Example trajectories of the upper sphere generated using the analytic solution and the TC-BEM for the case of $\Delta z_{-\infty}/a = 0.2$ and particle roughness $\epsilon/a = 1.0 \times 10^{-3}$ are shown in figure 3. In this case of linear shear flow, the trajectory of the lower sphere is the mirror image of the upper sphere. As seen in the figure, there is excellent agreement between the trajectory generated using the TC-BEM and the analytically generated trajectory (da Cunha & Hinch 1996). The particle separation, δ/a, as a function of far-field strain is shown in figure 4. Again, there is excellent agreement between the TC-BEM and the analytic solution. Both curves bottom out at a separation of $\delta/a = 1.03 \times 10^{-3}$ as dictated by the roughness model.

The difference in the upstream and downstream vertical separation of the centre of the spheres, $\Delta z_{\pm\infty} = \Delta z_{\infty} - \Delta z_{-\infty}$, is an important quantity in determining the particle self-diffusivity. In fact, the square of this quantity is used to calculate the in-plane self-diffusivity (da Cunha & Hinch 1996). For the case shown in figure 3, assuming the analytic model with roughness to be correct, the relative error in $(\Delta z_{\pm\infty})^2$ using the TC-BEM is 2.25 %. Hence, the TC-BEM can be used to obtain quantitatively correct self-diffusivities.

https://doi.org/10.1017/S0022112007000043 Published online by Cambridge University Press

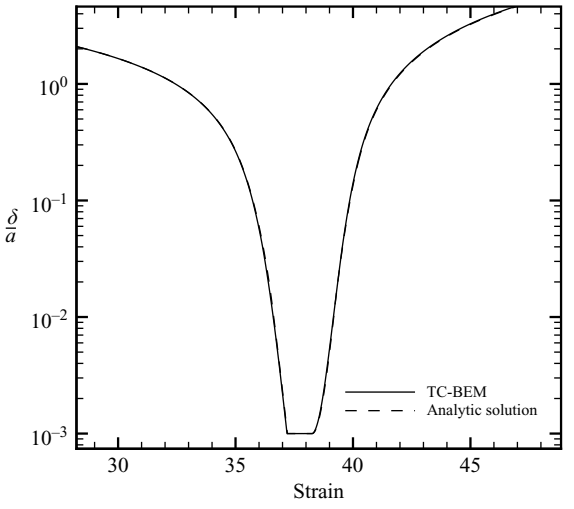


FIGURE 4. Particle separations as a function of strain for the case $\Delta z_{-\infty}/a = 0.2$ and $\epsilon/a = 1.0^{-3}$.

$\Delta z_{-\infty}/a$	$\Delta z_{\infty}/a$					
	$\epsilon/a = 1.0 \times 10^{-3}$		$\epsilon/a = 1.0 \times 10^{-4}$		$\epsilon/a = 0.0$	
	TC-BEM	Analytic	TC-BEM	Analytic	TC-BEM	Analytic
0.20	0.7146	0.7100	0.3470	0.3398	0.2034	0.2000
0.30	0.7146	0.7100	0.3456	0.3398	0.3018	0.3002
0.40	0.7146	0.7100	0.4004	0.4000	0.4004	0.4000
0.50	0.7146	0.7100	0.5002	0.5000	0.5002	0.5000
0.60	0.7146	0.7100	0.6004	0.6000	0.6004	0.6000
0.70	0.7146	0.7100				
0.72	0.7200	0.7200				
0.80	0.8000	0.8000				
1.00	1.0000	1.0000				

TABLE 1. Upstream ($\Delta z_{-\infty}/a$) and downstream ($\Delta z_{\infty}/a$) vertical separation of the centres of the spheres.

A number of additional cases are considered and the results for $\Delta z_{\infty}/a$ are shown in Table 1 for $\epsilon/a = 1.0 \times 10^{-3}$, $\epsilon/a = 1.0 \times 10^{-4}$, and smooth particles ($\epsilon/a = 0.0$). For the case of $\epsilon/a = 1.0 \times 10^{-3}$ with upstream vertical separations ranging from $0.2 \leqslant \Delta z_{-\infty}/a \leqslant 0.7$, the downstream vertical separation, $\Delta z_{\infty}/a$, as calculated by the TC-BEM is $\Delta z_{\infty}/a = 0.7146$ and as calculated using the analytical method is $\Delta z_{\infty}/a = 0.7100$. That is, for cases in which the initial vertical separations of the spheres is less than approximately 0.72, the trajectories of the particles are essentially the same after they pass one another. In fact, for both the TC-BEM and the analytical method, the roughness model is not invoked for $\Delta z_{-\infty}/a \geqslant 0.72$, and hence, the trajectories are essentially reversible, as evidenced by the fact that $\Delta z_{\pm\infty}/a = 0$. Similar results are seen in the table for the case $\epsilon/a = 1.0 \times 10^{-4}$. The final differences in the elevations of the spheres, $\Delta z_{\infty}/a$, do not change for the TC-BEM and analytic results for the irreversible cases in which $z_{-\infty}/a < 0.4$. The TC-BEM and analytic results are essentially reversible for $\Delta z_{-\infty}/a \geqslant 0.4$. Finally, the results for smooth

https://doi.org/10.1017/S0022112007000043 Published online by Cambridge University Press

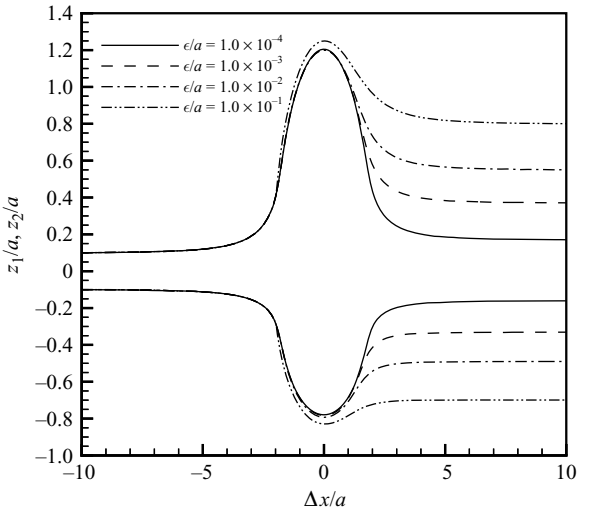


FIGURE 5. Typical TC-BEM-simulated trajectories in the shear plane of two rough spheres suspended in a nonlinear shear flow with initial positions $(-5.0, 0.05, 0.1)$ and $(5.0, -0.05, -0.1)$ and nonlinearity parameter $a\nabla\dot{\gamma}/\dot{\gamma} = 1.0$.

spheres show the high level of accuracy of the TC-BEM in that the predicted trajectories are essentially reversible despite the very narrow particle separations that occur during the simulations. It should be noted that a combination of mode I, mode II, and mode IV relative motions are simultaneously present during these simulations.

5. Self-diffusivity and migration of particle pairs

The self-diffusivity and migration of particle pairs is characterized by simulating the interaction of spheres suspended in nonlinear shear flows at a variety of relative initial positions. The far-field quadratic velocity profile is in the x-direction and is given by

$$u = b - c*(z-d)^2, \tag{5.1}$$

where b, c, and d are constants. Hence, the shear plane is the $x-z$ plane and the out-of-shear (vorticity) plane is the $x-y$ plane. The strength of the nonlinear flow is characterized by the nonlinearity parameter defined by $a\nabla\dot{\gamma}/\dot{\gamma}$.† As in the previous section, the simulations are started with $\Delta x_{-\infty}/a = -10$ and stopped when $\Delta x_{\infty}/a = 10$.

Typical BEM-simulated transient trajectories of particle pairs in the shear plane, in the out-of-shear plane, and the location of the centre of gravity in the shear plane are shown in figures 5–7, respectively, for particle roughnesses in the range of $1\times10^{-4} \leqslant \epsilon/a \leqslant 1\times10^{-1}$ and nonlinearity parameter $a\nabla\dot{\gamma}/\dot{\gamma} = 1.0$. The initial positions of the spheres are at $(-5.0,\ 0.05,\ 0.1)$ and $(5.0, -0.05, -0.1)$. As seen in figure 5, for the trajectories in the shear plane, neither sphere returns to its initial streamline after interaction, indicating that the trajectories are irreversible as in the case for linear shear flows. However, unlike the linear shear flow case, the trajectories become

† For the Poiseuille flow considered herein, the nonlinearity parameter takes on a particularly simple form, namely, $a\nabla\dot{\gamma}/\dot{\gamma} = a/(z-d)$, as determined from (5.1). However, for other flow fields such as circular Couette flow, the functional form is typically more complex.

https://doi.org/10.1017/S0022112007000043 Published online by Cambridge University Press

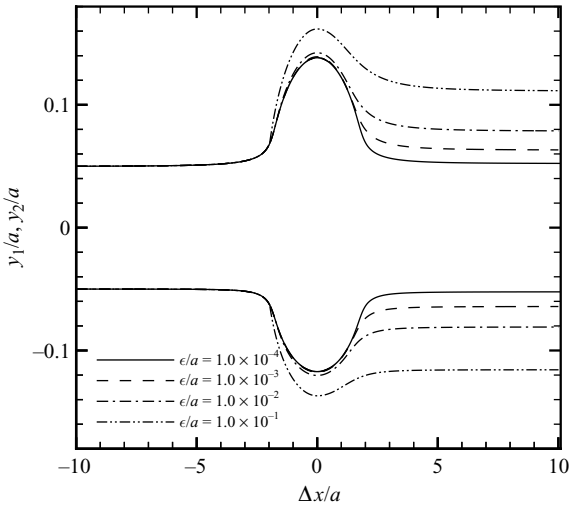


FIGURE 6. Typical TC-BEM-simulated trajectories in the out-of-shear plane of two rough spheres suspended in a nonlinear shear flow with initial positions $(-5.0, 0.05, 0.1)$ and $(5.0, -0.05, -0.1)$ and nonlinearity parameter $a\nabla\dot{\gamma}/\dot{\gamma} = 1.0$.

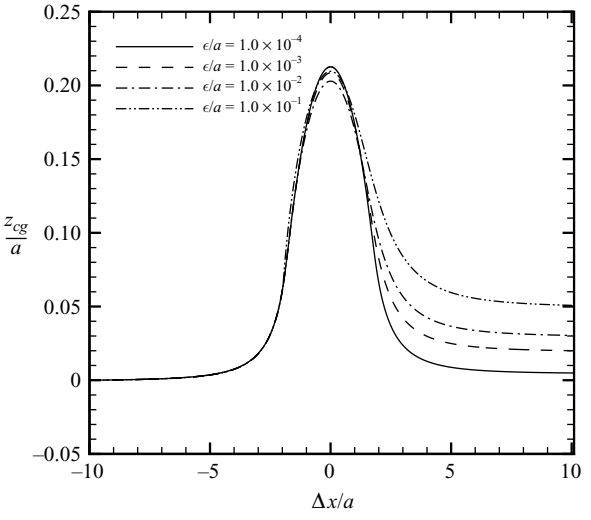


FIGURE 7. The vertical location of the centre of gravity, z_{cg}/a, as a function of $\Delta x/a$ for two rough spheres suspended in a nonlinear shear flow with initial positions $(-5.0, 0.05, 0.1)$ and $(5.0, -0.05, -0.1)$ and nonlinearity parameter $a\nabla\dot{\gamma}/\dot{\gamma} = 1.0$.

more and more asymmetric about the z-axis with increasing particle roughness. The characteristics of the trajectories in the out-of-shear plane (figure 6) are similar to the in-shear plane, including the loss of symmetry caused by the nonlinearity of the flow field. The asymmetries seen in the trajectories indicate that there is a net permanent displacement of the centre of gravity of the particle pair. The net displacement in the z-direction is always towards the low-shear-rate region of the flow field, and hence will be called particle migration. The net displacement in the y-direction will change sign with the sign of $\Delta y_{-\infty}$, and hence, when integrated over all possible relative starting positions of the particle pairs, will produce no net effect. The net permanent migration of the centre of gravity of the particle pair in the z-direction, $\Delta z_{cg}/a$, as shown in figure 7, is seen to increase with increasing particle roughness.

https://doi.org/10.1017/S0022112007000043 Published online by Cambridge University Press

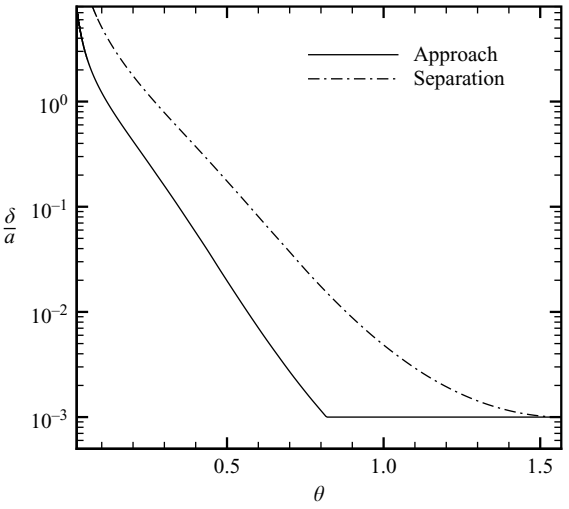


FIGURE 8. The inter-particle separation as a function of the angle made between the line of centres between the two spheres and the horizontal, θ, upon approach and separation for initial positions $(-5.0,\ 0.05,\ 0.1)$ and $(5.0,\ -0.05,\ -0.1)$, nonlinearity parameter $a\nabla\dot{\gamma}/\dot{\gamma} = 1.0$ and $\epsilon/a = 1.0 \times 10^{-3}$.

To better explain the underlying cause of the migration of the centre of gravity of the particle pair to the low-shear- rate region of the flow field, a plot of the inter-particle separation between the two spheres, δ/a, for the case $\epsilon/a = 1.0 \times 10^{-3}$ as a function of the angle that the line of centres of the spheres make with the horizontal (x-axis) upon approach and separation, is shown in figure 8. As has been noted by a variety of researchers (da Cunha & Hinch 1996; Rampall, Smart & Leighton 1997; Morris & Boulay 1999), roughness disturbs the symmetry of the interaction and, as can be seen in the figure, the particle separation is significantly larger on separation compared to on approach. However, there is an important ancillary effect caused by the asymmetry in the inter-particle separations upon approach and separation. This effect is shown in figure 9, where the absolute value of the average vertical velocity (z-direction) of the particle pair, $|w_{cg}|$, is plotted again as a function of the angle that the line-of-centres of the spheres make with the horizontal. On approach, the particle pair moves towards the lower-shear-rate region of the flow field and, on separation, the particle pair moves back towards the higher-shear-rate region of the flow field. However, the movement during separation is generally slower than during approach, causing a net permanent displacement of the centre of gravity of the particle pair.

To further reinforce the basis for the migration of a pair of rough spheres in nonlinear shear flow caused by the asymmetry in inter-particle separations upon approach and separation, a sequence of snapshots is considered of two particles suspended in a nonlinear shear flow with a fixed centre of gravity but with a variety of surface-to-surface separations δ. For the particular case considered, the nonlinearity parameter is given by $a\nabla\dot{\gamma}/\dot{\gamma} = 1.0$. At the farthest separation, the locations of the two particles are given in units of particle radius by (11.45052, 0.10728, 0.86701) and (12.82163, −0.0947509, −0.58903) with the inter-particle separation given by $\delta/a = 1.01832 \times 10^{-2}$. At this location, the z-component of velocity of the first particle is given by $w_1 = 0.36059$ and the z-component of velocity of the second particle is given by $w_2 = -0.22716$. Hence, the centre of gravity of the particle pair is migrating towards the low-shear-rate region of the flow field with velocity $w_{cg} = 0.066715$. Now,

https://doi.org/10.1017/S0022112007000043 Published online by Cambridge University Press

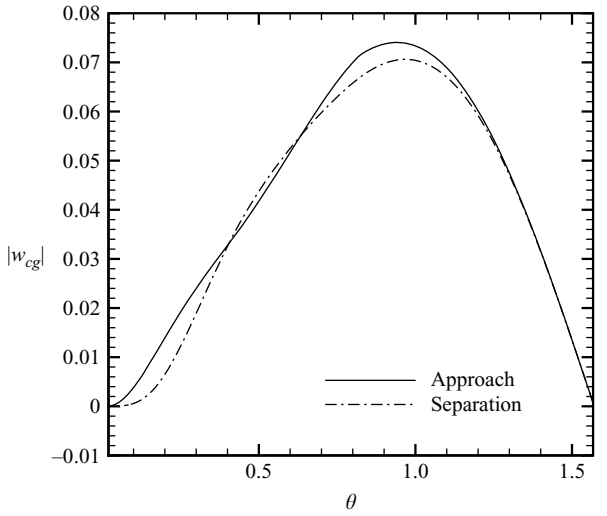


FIGURE 9. The average absolute value of the vertical velocity of the particle pair, $|w_{cg}|$, as a function of the angle made between the line of centres between the two spheres and the horizontal, θ, upon approach and separation for initial positions $(-5.0, 0.05, 0.1)$ and $(5.0, -0.05, -0.1)$, nonlinearity parameter $a\nabla\dot{\gamma}/\dot{\gamma} = 1.0$ and $\epsilon/a = 1.0 \times 10^{-3}$.

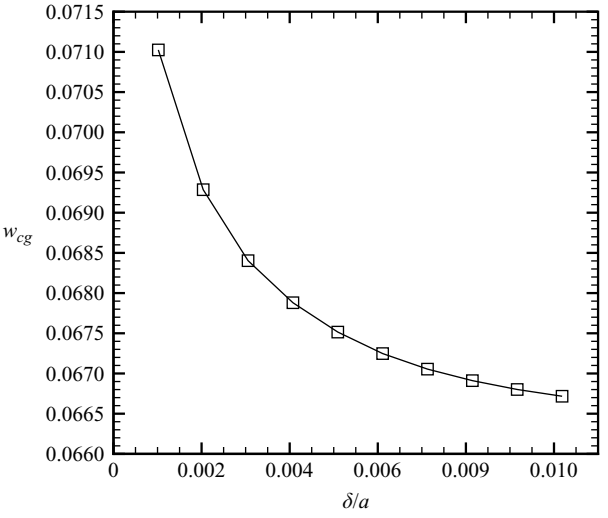


FIGURE 10. The average vertical velocity of the particle pair as a function of inter-particle separation.

additional snapshots are taken after perturbing the particles inward towards each other along their line of centres. A plot of the velocity of the centre of gravity w_{cg} as a function of separation δ/a is shown in figure 10. The migration velocity is seen to decrease with increasing separation. If the particles were perfectly smooth, the particle trajectories would be perfectly symmetric upon approach and separation. At a certain location upon approach, the particles would move towards the low-shear-rate region of the flow field with a given speed. At the symmetric point during separation, the particles would be exactly the same distance apart, and hence the particle pair would

https://doi.org/10.1017/S0022112007000043 Published online by Cambridge University Press

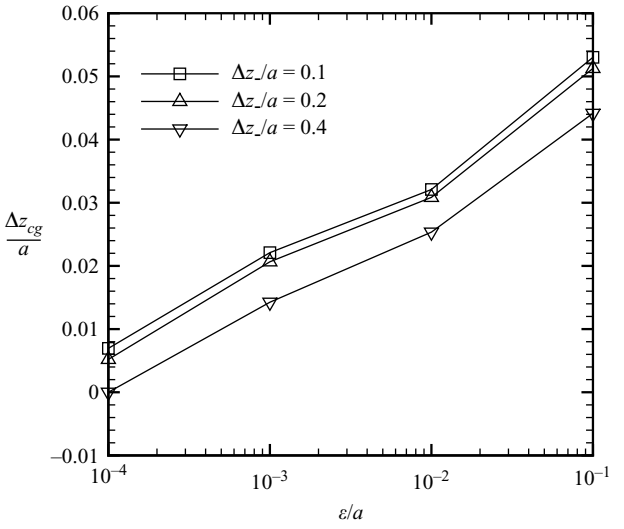


FIGURE 11. The effect of surface roughness ϵ and the initial particle separation $\Delta z_{-\infty}$ on the net permanent displacement of the centre of gravity of the particle pair for the case $\Delta y_{-\infty}/a = 0$ and $a\nabla\dot{\gamma}/\dot{\gamma} = 1.0$.

move towards the high-shear-rate region of the flow field with exactly the same speed as upon approach. Hence, after separation, there would be no net migration of the particle pair. However, for rough particles, the distance between the particles on separation is greater than on approach, and hence the speed at which the particles move towards the low-shear-rate region on approach is faster than the speed at which the particles move towards the high-shear-rate region on separation. Therefore, the net effect is the observed migration of the particle pair towards the low-shear-rate region of the flow field.

The net permanent displacement of the centre of gravity of rough particle pairs in nonlinear shear flows is shown as a function of surface roughness in figure 11 for a variety of initial vertical displacements and in figure 12 for a variety of values of the nonlinearity parameter. The net permanent displacement of the centre of gravity is seen to increase with increasing particle roughness and nonlinearity parameter but decrease with increasing initial vertical separation. In fact, the net permanent displacement increases essentially linearly with increasing nonlinearity parameter, as seen in figure 13.

The self-diffusivity of a single, marked particle in a suspension undergoing shear flow is defined as half the rate of change in time of the variance of the displacement of the cross-streamline random walk due to collisions with other particles. The dilute suspension under consideration is at a uniform concentration with $\phi = \frac{4}{3}\pi n a^3 \ll 1$, where n is the number density of the particles in the suspension. Following da Cunha & Hinch (1996), the rate of collisions with relative displacements in $(y_{-\infty}, y_{-\infty} + \delta y_{-\infty}) \times (z_{-\infty}, z_{-\infty} + \delta z_{-\infty})$, which have spheres approaching at a relative velocity of $\Delta v_{-\infty}$, is $n\Delta v_{-\infty}\delta y_{-\infty}\delta z_{-\infty}$. A collision with these parameters produces net displacements of the test sphere $(-\Delta y_{\pm\infty}, -\Delta z_{\pm\infty})$. As it is assumed that each of these collisions is uncorrelated, the self-diffusivities in the z-direction can be calculated by

$$D_z^s = \frac{1}{2}\int_{-\infty}^{\infty}\int_{-\infty}^{\infty}(\Delta z_{\pm\infty})^2 n\Delta v_{-\infty}\,\mathrm{d}y_{-\infty}\,\mathrm{d}z_{-\infty}. \tag{5.2}$$

https://doi.org/10.1017/S0022112007000043 Published online by Cambridge University Press

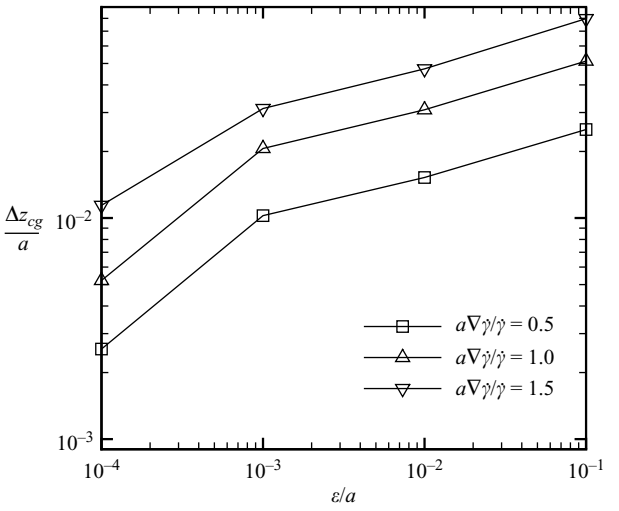


FIGURE 12. The effect of surface roughness ϵ and the nonlinearity parameter $a\nabla\dot{\gamma}/\dot{\gamma}$ on the net permanent displacement of the centre of gravity of the particle pair Δz_{cg} for the case $\Delta y_{-\infty}/a = 0$ and $\Delta z_{-\infty} = 0.2$.

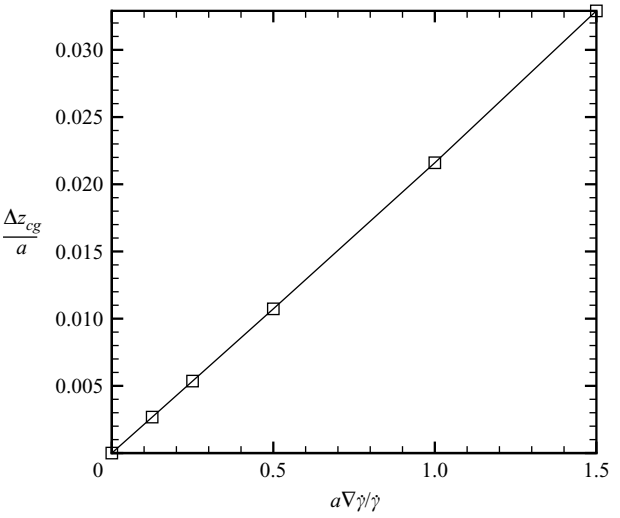


FIGURE 13. The net permanent displacement of the particle pair Δz_{cg} as a function of the nonlinearity parameter $a\nabla\dot{\gamma}/\dot{\gamma}$ for a roughness of $\epsilon/a = 1.0 \times 10^{-3}$. The initial particle separations are given by $\Delta y_{-\infty}/a = 0.076637$ and $\Delta z_{-\infty}/a = 0.056351$.

Non-dimensionalizing the lengths in the integral with the radius of the sphere, a, yields

$$D_z^s = \phi a^2 \frac{3}{8\pi} \int_{-\infty}^{\infty} \int_{-\infty}^{\infty} (\Delta z_{\pm\infty})^2 \Delta v_{-\infty} \, \mathrm{d}y_{-\infty} \, \mathrm{d}z_{-\infty}. \tag{5.3}$$

Now, for the Poiseuille flow under consideration with far-field velocity given by (5.1), it can be shown that

$$\Delta v_{-\infty} = \dot{\gamma}_{cg} \Delta z_{-\infty}, \tag{5.4}$$

https://doi.org/10.1017/S0022112007000043 Published online by Cambridge University Press

$a\nabla\dot{\gamma}/\dot{\gamma}$	$D_y^s/\phi a^2\dot{\gamma}$	$D_z^s/\phi a^2\dot{\gamma}$
0.0	0.1330×10^{-4}	0.8653×10^{-3}
0.125	0.1342×10^{-4}	0.8692×10^{-3}
0.25	0.1341×10^{-4}	0.8689×10^{-3}
0.5	0.1339×10^{-4}	0.8680×10^{-3}
1.0	0.1322×10^{-4}	0.8627×10^{-3}
1.5	0.1317×10^{-4}	0.8595×10^{-3}

TABLE 2. The self-diffusivity coefficients divided by $\phi a^2\dot{\gamma}$ as a function of the nonlinearity parameter for the case $\epsilon/a = 1.0\times10^{-3}$.

where $\dot{\gamma}_{cg}$ is the shear rate at the centre of gravity of the particle pair before interaction. Hence, the self-diffusivity in the z-direction is given by

$$D_z^s = \phi a^2\dot{\gamma}\frac{3}{8\pi}\int_{-\infty}^{\infty}\int_{-\infty}^{\infty}(\Delta z_{\pm\infty})^2\Delta z_{-\infty}\,\mathrm{d}y_{-\infty}\,\mathrm{d}z_{-\infty}. \tag{5.5}$$

The self-diffusivity in the y-direction, D_y^s, can be derived in a similar manner and is given by

$$D_y^s = \phi a^2\dot{\gamma}\frac{3}{8\pi}\int_{-\infty}^{\infty}\int_{-\infty}^{\infty}(\Delta y_{\pm\infty})^2\Delta z_{-\infty}\,\mathrm{d}y_{-\infty}\,\mathrm{d}z_{-\infty}. \tag{5.6}$$

These formulas for the self-diffusivity reduce to those given by da Cunha & Hinch (1996) for a linear shear flow.

The net displacement of the centre of gravity of the particle pair can be characterized by a migration diffusion coefficient, D^m, defined by

$$D^m = \phi a^2\dot{\gamma}\frac{3}{8\pi}\int_{-\infty}^{\infty}\int_{-\infty}^{\infty}(\Delta z_{cg})^2\Delta z_{-\infty}\,\mathrm{d}y_{-\infty}\,\mathrm{d}z_{-\infty}. \tag{5.7}$$

Hence, the migration diffusion coefficient measures the variance of the location of the centre of gravity caused by the two-particle interactions. However, unlike the self-diffusivity coefficients D_y^s and D_z^s, there is an associated directionality of the migration towards the low-shear-rate region of the flow field.

The three diffusivities, D_z^s, D_y^s, and D^m, are evaluated numerically based on the TC-BEM simulations. The integration is performed over the positive quadrant and, by symmetry, that result is quadrupled to determine the diffusivities. A plot of $D_z^s/\phi a^2\dot{\gamma}$ and $D_y^s/\phi a^2\dot{\gamma}$ for the case $a\nabla\dot{\gamma}/\dot{\gamma} = 1.0$ is shown in figure 14. These results actually match those of da Cunha & Hinch (1996) quite well, despite the fact that da Cunha & Hinch performed their simulations in a linear shear flow. Even though the trajectories of the particles are quite different in linear and nonlinear shear flows, the net change in the spread in the y- and z-directions between the centres of the particles as characterized by $\Delta y_{\pm\infty}$ and $\Delta z_{\pm\infty}$ is remarkably unaffected. To reinforce this point, the self-diffusivities are shown in table 2 for a variety of values of the nonlinearity parameter including $a\nabla\dot{\gamma}/\dot{\gamma} = 0.0$, (i.e. for a linear shear flow), with roughness given by $\epsilon/a = 1.0\times10^{-3}$. It is seen in the table that the self-diffusivities are essentially constant. Similar results were obtained for other values of roughness.

The migration diffusion coefficient D^m divided by $\phi a^2\dot{\gamma}$ is shown in figure 15 as a function of the nonlinearity parameter for a variety of particle roughnesses. The trends are the same as those discussed above for the net displacement of the centre

https://doi.org/10.1017/S0022112007000043 Published online by Cambridge University Press

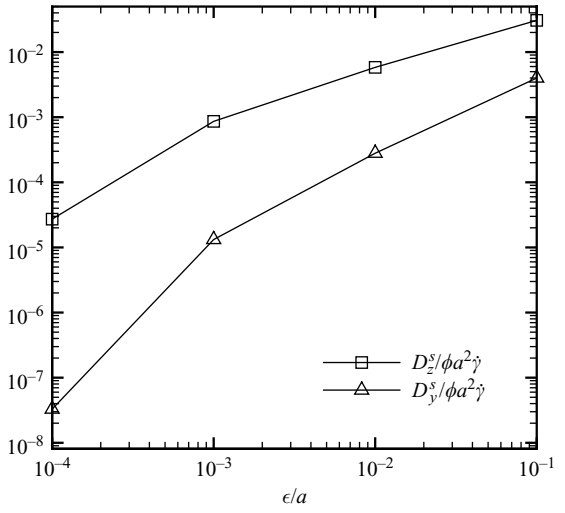


FIGURE 14. The self-diffusivity coefficients, D_z^s and D_y^s divided by $\phi a^2\dot{\gamma}$, for dilute suspensions of rough spheres suspended in a nonlinear shear flow for the case $a\nabla\dot{\gamma}/\dot{\gamma} = 1.0$.

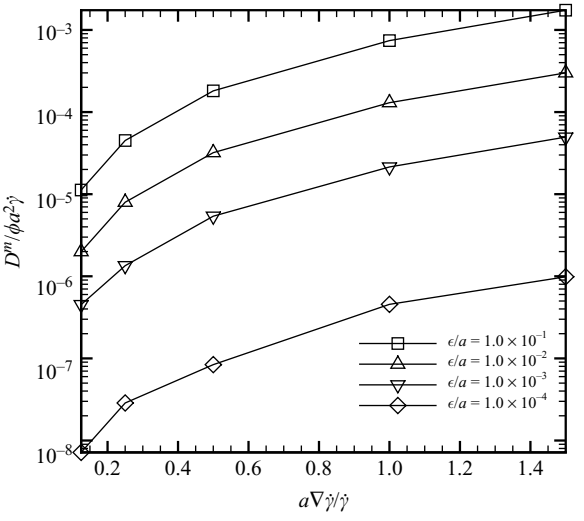


FIGURE 15. The migration diffusivity coefficient, D^m divided by $\phi a^2\dot{\gamma}$, as a function of the nonlinearity parameter.

of gravity of the particle pair in nonlinear shear flow. That is, the migration diffusion coefficient increases with both the particle roughness and the nonlinearity parameter.

6. Conclusions

The analysis of self-diffusion and migration of rough spheres in nonlinear shear flows at negligible Reynolds numbers is performed using a traction-corrected boundary element method (TC-BEM). The TC-BEM is based on coupling the asymptotic traction solution in the interstitial region between particles with boundary element equations for the fluid and kinematic and equilibrium equations for the

https://doi.org/10.1017/S0022112007000043 Published online by Cambridge University Press

particles. The resulting system is fully coupled through the particle velocities. The asymptotic traction solution presented in this work is new and should have additional applications. The current numerical approach is substantially different from previous numerical techniques based on lubrication forces and moments. Although these previous methods could resolve gross features of the flow field, they are inadequate for following individual particle trajectories, and hence cannot be used to determine diffusivities of dilute suspensions. The TC-BEM was benchmarked against analytic solutions and was shown to be extremely accurate even for small inter-particle separations.

The main result of the current study is that there is a net migration of the centre of gravity of a pair of rough spheres suspended in a nonlinear shear flow towards the low-shear-rate region of the flow. This migration increases with the nonlinearity of the flow field and with particle roughness. A detailed explanation is provided for the particle migration based on the fact that the speed of the centre of gravity towards (upon approach) or away (upon separation) from the low-shear-rate region of the flow field is a function of inter-particle separation. Roughness causes inter-particle separations to be larger during separation compared to approach, which causes the permanent net migration of the centre of gravity of the particle pair towards the lower-shear-rate region.

The particle self-diffusivity coefficients, D_y^s and D_z^s, were calculated over a range of roughnesses and nonlinear parameters. For linear shear flows, the current results determined using the TC-BEM matched analytic results. Interestingly, it was determined that the self-diffusivities are not functions of the nonlinearity parameter. A new migration diffusivity, D^m, was defined to characterize the variance of the net displacement of the centre of gravity of a particle pair. The migration diffusivity increased with both particle roughness and the nonlinearity parameter. In fact, for large values of the nonlinearity parameter, the migration diffusivity could actually exceed the out-of-plane self-diffusivity.

The migration of a rough particle pair towards the low-shear-rate region of the flow field is a significant new result of this research because it provides a clue as to why current rheological models for suspension flows are inadequate in modelling transient concentration profiles. Most explanations for particle migration upon which these models are based discuss asymmetrical multi-body interactions associated with gradients in shear rate, concentration, effective suspension viscosity, and/or particle-phase stress. However, no rheological model proposed to date can model the transient experimental data collected in Couette devices, eccentric bearing geometries, pipe flow, expansion flow, among others. In fact, the current models are typically orders of magnitude off in predicting the time to steady state. As an example, consider a suspension flow in a Couette device of fixed dimensions with the inner cylinder rotating and the outer cylinder fixed. The current rheological models predict the migration rate to scale with the square of the characteristic particle radius. On the other hand, experimental data suggest that the migration scales with the particle radius raised by a power anywhere from 2.5 to 2.9. However, this new mechanism for the net migration of rough particle pairs detailed in this research is missing from these models. It has been shown in the current study that the magnitude of the net permanent displacement of the centre of gravity of a pair of interacting particles essentially scales linearly with the nonlinearity parameter. Since the mean flow profile in the Couette device does not change significantly with particle size, the nonlinearity parameter also increases linearly with particle radius. This then suggests that the diffusion coefficients themselves used in the current rheological models should be

https://doi.org/10.1017/S0022112007000043 Published online by Cambridge University Press

functions of the nonlinearity parameter to account for the enhanced migration of particle pairs during interaction caused by the nonlinearity of the flow field itself. Our research group is currently investigating incorporating a functional dependence of the diffusion coefficients on the nonlinearity parameter in these rheological models.

This work was partially supported by the US Department of Energy (DOE) grant DE-FG02-05ER25705. This financial support does not constitute an endorsement by the DOE of the views expressed in this paper. Los Alamos National Laboratory, an affirmative action/equal opportunity employer, is operated by the Los Alamos National Security, LLC for the National Nuclear Security Administration of the US Department of Energy under contract DE-AC52-06NA25396. This material was based on work supported by the National Science Foundation, while Marc Ingber was working at the Foundation.

Appendix A. Mode I motion

The asymptotic velocity and pressure fields for mode I motion are given by:

$$
\begin{aligned}
u = \frac{a^5\cos(\theta)}{3000(a^5r^2+\delta)^5}\Bigg(&180r^{12}+\left(1000z+\frac{469\delta}{a}-150\right)r^{10}\\
&+\left(1980z^2+20\left(\frac{101\delta}{a}-150\right)z-\delta\left(\frac{4247\delta}{a^2}+\frac{1050}{a}\right)\right)r^8\\
&+\left(5000z^3+24\left(\frac{211\delta}{a}-225\right)z^2-24\delta\left(\frac{86\delta}{a^2}+\frac{275}{a}\right)z-10\delta^2\left(\frac{673\delta}{a^3}+\frac{405}{a^2}\right)\right)r^6\\
&+10\Bigg(-\frac{1700\delta z^3}{a}+12\delta\left(\frac{403\delta}{a^2}-\frac{75}{a}\right)z^2-4\delta^2\left(\frac{884\delta}{a^3}+\frac{225}{a^2}\right)z\\
&+5\delta^3\left(\frac{145\delta}{a^4}-\frac{111}{a^3}\right)+1200z^4\Bigg)r^4-100\delta\left(\frac{408z^4}{a}-\frac{806\delta z^3}{a^2}+3\delta\left(\frac{187\delta}{a^3}+\frac{6}{a^2}\right)z^2\right.\\
&\left.+\delta^2\left(\frac{102}{a^3}-\frac{193\delta}{a^4}\right)z-3\delta^3\left(\frac{\delta}{a^5}-\frac{8}{a^4}\right)\right)r^2\\
&+600z\delta^2\left(\frac{8z^3}{a^2}-\frac{21\delta z^2}{a^3}+3\delta\left(\frac{4\delta}{a^4}+\frac{1}{a^3}\right)z+\delta^2\left(\frac{\delta}{a^5}-\frac{8}{a^4}\right)\right)\Bigg),
\end{aligned}
\tag{A 1}
$$

$$
\begin{aligned}
v = \frac{a^4\sin(\theta)}{3000(a^4r^2+\delta)^4}\Bigg(&-1170r^{10}+\left(-2000z-\frac{4217\delta}{a}+1950\right)r^8\\
&+6\left(330z^2+\left(500-\frac{1330\delta}{a}\right)z+\delta\left(\frac{1050}{a}-\frac{1109\delta}{a^2}\right)\right)r^6\\
&-2\Bigg(500z^3+\left(900-\frac{3954\delta}{a}\right)z^2+6\delta\left(\frac{1159\delta}{a^2}-\frac{900}{a}\right)z+25\delta^2\left(\frac{101\delta}{a^3}-\frac{135}{a^2}\right)\Bigg)r^4\\
&+100\Bigg(24z^4-\frac{28\delta z^3}{a}+3\delta\left(\frac{41\delta}{a^2}-\frac{12}{a}\right)z^2+\delta^2\left(\frac{126}{a^2}-\frac{149\delta}{a^3}\right)z-3\delta^3\left(\frac{\delta}{a^4}-\frac{8}{a^3}\right)\Bigg)r^2\\
&-600z\delta\left(\frac{8z^3}{a}-\frac{21\delta z^2}{a^2}+3\delta\left(\frac{4\delta}{a^3}+\frac{1}{a^2}\right)z+\delta^2\left(\frac{\delta}{a^4}-\frac{8}{a^3}\right)\right)\Bigg),
\end{aligned}
\tag{A 2}
$$

https://doi.org/10.1017/S0022112007000043 Published online by Cambridge University Press

$$
\begin{aligned}
w = \frac{a^6 r\cos(\theta)}{3000(ar^2+\delta)^6}\Bigg(&\left(630z-\frac{65\delta}{a}-750\right)r^{12}\\
&+\left(500z^2+4\left(\frac{937\delta}{a}-450\right)z-\frac{\delta}{a}\left(\frac{2461\delta}{a}+3600\right)\right)r^{10}\\
&+3\left(500\left(\frac{\delta}{a}-2\right)z^2+\frac{4\delta z}{a}\left(\frac{571\delta}{a}-800\right)-\frac{\delta^2}{a^2}\left(\frac{5057\delta}{a}+1900\right)\right)r^8\\
&+\left(4000z^4-32\left(\frac{151\delta}{a}+150\right)z^3+\frac{4\delta z^2}{a}\left(\frac{937\delta}{a}-1200\right)\right.\\
&\left.+\frac{96\delta^2 z}{a^2}\left(\frac{423\delta}{a}-250\right)-\frac{5\delta^3}{a^3}\left(\frac{9871\delta}{a}+240\right)\right)r^6\\
&+2\left(5760z^5-\frac{14400\delta z^4}{a}+\frac{29376\delta^2 z^3}{a^2}-\frac{2\delta^2 z^2}{a^2}\left(\frac{13957\delta}{a}+4500\right)\right.\\
&\left.+\frac{\delta^3 z}{a^3}\left(\frac{50207\delta}{a}-10800\right)+\frac{\delta^4}{a^4}\left(2025-\frac{33854\delta}{a}\right)\right)r^4\\
&-\frac{12r^2\delta}{a}\left(5760z^5-\frac{13400\delta z^4}{a}+\frac{8\delta z^3}{a}\left(\frac{2291\delta}{a}-150\right)\right.\\
&\left.+\frac{2\delta^2 z^2}{a^2}\left(1400-\frac{7421\delta}{a}\right)+\frac{25\delta^3 z}{a^3}\left(\frac{95\delta}{a}+2\right)+\frac{8\delta^4}{a^4}\left(\frac{188\delta}{a}-25\right)\right)\\
&+\frac{40\delta^2}{a^2}\left(864z^5-\frac{2360\delta z^4}{a}+\frac{40\delta z^3}{a}\left(\frac{49\delta}{a}+6\right)-\frac{5\delta^2 z^2}{a^2}\left(\frac{91\delta}{a}+87\right)\right.\\
&\left.-\frac{15\delta^3 z}{a^3}\left(\frac{\delta}{a}-8\right)+\frac{6\delta^5}{a^5}\right)\Bigg),
\end{aligned}
\tag{A 3}
$$

$$
\begin{aligned}
p = -\frac{1}{125(ar^2+\delta^2)^4}&(ar\sqrt{\delta}(-200\delta^6+25a(17r^2+58z-6\delta)\delta^4-a^2(41r^4\\
&+100(z+3\delta)r^2+1200z^2)\delta^2+5a^3(3r^6+10(5z-3\delta)r^4+120z^2r^2))).
\end{aligned}
\tag{A 4}
$$

Appendix B. Mode II motion

The asymptotic velocity and pressure fields for mode II motion are given by:

$$
\begin{aligned}
u = \frac{a^3\cos(\theta)}{12(ar^2+\delta)^3}\Bigg(&\left(2z-\frac{\delta}{a}+6\right)r^6+2\left(\frac{\delta}{a}\left(6-\frac{\delta}{a}\right)+2z\left(\frac{\delta}{a}+3\right)\right)r^4\\
&+\left(-20z^3+\frac{30\delta z^2}{a}-\frac{8\delta}{a}\left(\frac{2\delta}{a}-3\right)z+\frac{3\delta^2}{a^2}\left(\frac{\delta}{a}+2\right)\right)r^2\\
&+\frac{6z\delta}{a}\left(2z^2-\frac{3\delta z}{a}+\frac{\delta}{a}\left(\frac{\delta}{a}+2\right)\right)\Bigg),
\end{aligned}
\tag{B 1}
$$

$$
\begin{aligned}
v = \frac{a^3\sin(\theta)}{12(ar^2+\delta)^3}\Bigg(&\left(2z-\frac{\delta}{a}-6\right)r^6+2\left(2z\left(\frac{\delta}{a}-3\right)-\frac{\delta}{a}\left(\frac{\delta}{a}+6\right)\right)r^4\\
&+\left(4z^3-\frac{6\delta z^2}{a}+\frac{8\delta z}{a}\left(\frac{\delta}{a}-3\right)-\frac{3\delta^2}{a^2}\left(\frac{\delta}{a}+2\right)\right)r^2\\
&-\frac{6z\delta}{a}\left(2z^2-\frac{3\delta z}{a}+\frac{\delta}{a}\left(\frac{\delta}{a}+2\right)\right)\Bigg),
\end{aligned}
\tag{B 2}
$$

https://doi.org/10.1017/S0022112007000043 Published online by Cambridge University Press

$$w = \frac{a^4 r\cos(\theta)}{24(ar^2+\delta)^4}\left(\left(\frac{\delta}{a}-6\right)r^8 + \left(-4z^2 + \frac{4\delta z}{a} + \frac{3\delta}{a}\left(\frac{\delta}{a}-8\right)\right)r^6 - 2\left(4\left(\frac{2\delta}{a}-3\right)z^2 + \frac{4\delta z}{a}\left(3-\frac{2\delta}{a}\right) - \frac{\delta^2}{a^2}\left(\frac{\delta}{a}-15\right)\right)r^4 - 2\left(16z^4 - \frac{32\delta z^3}{a} + \frac{8\delta z^2}{a}\left(\frac{5\delta}{a}-3\right) - \frac{24\delta^2 z}{a^2}\left(\frac{\delta}{a}-1\right) + \frac{3\delta^3}{a^3}\left(\frac{\delta}{a}+2\right)\right)r^2 + \frac{4z\delta}{a}\left(16z^3 - \frac{32\delta z^2}{a} + \frac{\delta z}{a}\left(\frac{19\delta}{a}+6\right) - \frac{3\delta^2}{a^2}\left(\frac{\delta}{a}+2\right)\right)\right), \tag{B 3}$$

$$p = \frac{ar\sqrt{\delta}(2az-\delta^2)}{(ar^2+\delta^2)^2}. \tag{B 4}$$

Appendix C. Mode III motion

The asymptotic velocity and pressure fields for mode III motion are given by:

$$u = 0, \tag{C 1}$$

$$v = \frac{a(r^3+2zr)}{2(ar^2+\delta)}, \tag{C 2}$$

$$w = 0, \tag{C 3}$$

$$p = 0. \tag{C 4}$$

Appendix D. Mode IV motion

The asymptotic velocity and pressure fields for mode IV motion are given by:

$$u = 12r\left(r^2+\frac{\delta}{a}\right)\left(3r^5 + \frac{2\delta r^2}{a} + \frac{\delta^2}{a^2} - \frac{\sqrt{\delta}(2az+\delta)^2}{\sqrt{2}a^{3/2}}\right) - r^4\left(\sqrt{\frac{\delta}{2a}}\left(r^2+\frac{\delta}{a}\right)^2 - \frac{3(2az+\delta)^2}{a^2}\right)\left(16\left(r^2+\frac{\delta}{a}\right)\right)^{-4},$$

$$v = 0, \tag{D 1}$$

$$w = -\frac{1}{2} + \frac{3a^2(2az+\delta)((r^6-28r^2z^2)a^2 + (5r^4-28zr^2-12z^2)\delta a - 12z\delta^2)r^4}{16(ar^2+\delta)^5} - \frac{4(2az+\delta)(8r^2z^2a^3 + (3r^4+8zr^2-4z^2)\delta a^2 + 4(2r^2-z)\delta^2 a + 2\delta^3)}{16(ar^2+\delta)^4}, \tag{D 2}$$

$$p = -\frac{3a\left(a^2\left(3r^2-2\right)r^2 + \delta^2 + a\left(3r^2-2\right)\delta\right)}{4(ar^2+\delta)^3}. \tag{D 3}$$

REFERENCES

Abbott, J. R., Tetlow, N., Graham, A. L., Altobelli, S. A., Fukushima, E., Mondy, A. L. & Stephens, T. S. 1991 Experimental observation of particle migration in concentrated suspensions: Couette flow. *J. Rheol.* **35**, 773–795.

https://doi.org/10.1017/S0022112007000043 Published online by Cambridge University Press

Ascoli, E. P., Dandy, D. S. & Leal, L. G. 1989 Low Reynolds number hydrodynamic interaction of solid particle with planar wall. *Intl J. Numer. Meth. Fluids* **9**, 651–688.

Batchelor, G. K. & Green, J. T. 1972 The hydrodynamic interaction of two small freely-moving spheres in a linear flow field. *J. Fluid Mech.* **56**, 375–400.

Bossis, G. & Brady, J. F. 1984 Dynamic simulation of sheared suspensions. Part I. General method. *J. Chem. Phys.* **80**, 5141–5154.

Bossis, G. & Brady, J. F. 1987 Self-diffusion of Brownian particles in concentrated suspension under shear. *J. Chem. Phys.* **87**, 5437–5448.

Brady, J. F. & Bossis, G. 1985 The Rheology of concentrated suspensions of spheres in simple shear-flow by numerical simulation. *J. Fluid Mech.* **155**, 105–129.

Brady, J. F. & Morris, J. F. 1997 Microstructure of strongly shear suspensions and its impact on rheology and diffusion. *J. Fluid Mech.* **348**, 103–139.

Brenner, H. 1961 The slow motion of a sphere through a viscous fluid towards a planar surface. *Chem. Engng Sci.* **16**, 242–251.

Buyevich, I. A. 1995 Particle distribution in suspension shear flow. *Chem. Engng Sci.* **51**, 635–647.

Chan, C. Y., Beris, A. N. & Advani, S. G. 1992 Second order boundary element method calculations of hydrodynamic interactions between particles in close proximity. *Intl J. Numer. Meth. Fluids* **14**, 1063–1086.

Chang, C. & Powell, R. L. 1994 The rheology of bimodal hard-sphere dispersions. *Phys. Fluids* **6**, 1628–1636.

Cooley, M. D. & O'Neill, M. E. 1969 On the slow motion generated in a viscous fluid by the approach of a sphere to a plane wall or a stationary sphere. *Mathematika* **16**, 37–49.

Corless, R. M. & Jeffrey, D. J. 1988 Stress moments of nearly touching spheres in low Reynolds number flow. *Z. Angew. Math. Phys.* **39**, 874–884.

Cox, R. G. & Brenner, H. 1967 The slow motion of a sphere through a viscous fluid towards a plane surface. Part II. Small gap widths, including inertial effects. *Chem. Engng Sci.* **22**, 1753–1777.

da Cunha, F. R. & Hinch, E. J. 1996 Shear-induced dispersion in a dilute suspension of rough spheres. *J. Fluid Mech.* **309**, 211–223.

Dance, S. L. & Maxey, M. R. 2003 Incorporation of lubrication effects into the force-coupling method for particulate two-phase flow. *J. Comput. Phys.* **189**, 212–238.

Eckstein, E. C., Bailey, G. & Shapiro, A. H. 1977 Self-diffusion of particles in shear flow of a suspension. *J. Fluid Mech.* **79**, 191–208.

Fang, Z., Mammoli, A. A., Brady, J. F., Ingber, M. S., Mondy, L. A. & Graham, A. L. 2002 Flow-aligned tensor models for suspension flows. *Intl J. Mult. Flow* **28**, 137–166.

Graham, A. L. & Bird, R. B. 1984 Particle clusters in concentrated suspensions. Part 1. experimental-observations of particle clusters. *Ind. Engng Chem Fund.* **23**, 406–410.

Hampton, R. E., Mammoli, A. A. & Ingber, M. S. 2003 A corrected BEM for the inclusion of near-field effects associated with suspension flows at low Reynolds numbers. In *Boundary Element Technology XV* (ed. C. A. Brebbia & R. E. Dippery), pp. 249–258. WIT Press.

Hsiao, S.-C., Christensen, D., Ingber, M. S., Mondy, L. A. & Altobelli, S. A. 2003 Particle migration rates in a Couette apparatus. In *Computational Methods in Multiphase Flow II* (ed. C. A. Brebbia & A. A. Mammoli), pp. 241–251. WIT Press.

Ingber, M. S. 1989 Numerical simulation of the hydrodynamic interaction between a sedimenting particle and a neutrally buoyant particle. *Intl J. Num. Meth. Fluids* **9**, 263–273.

Ingber, M. S., Mammoli, A. A., Vorobieff, P., McCollum, T. & Graham, A. L. 2006 Experimental and numerical analysis of irreversibilities particles suspended in a Couette device. *J. Rheol.* **50**, 99–114.

Ingber, M. S., Subia, S. R. & Mondy, L. A. 2000 Massively parallel boundary element method modeling of particles in low-Reynolds number Newtonian fluid flows. In *Applications of High-Performance Computing in Engineering* (ed. M. S. Ingber, H. Power & C. A. Brebbia), pp. 313–324. WIT Press.

Jánosi, I. M., Tel, T., Wolf, D. E. & Garcia, J. A. C. 1997 Chaotic particle dynamics in viscous flows: The three particle Stokeslet problem. *Phys. Rev.* E **56**, 2858–2868.

Jayaweera, K. O. L. F., Mason, B. F. & Slack, G. W. 1964 The behaviour of clusters of spheres falling in a viscous fluid. *J. Fluid Mech.* **20**, 121–128.

https://doi.org/10.1017/S0022112007000043 Published online by Cambridge University Press

Jeffrey, D. J. & Onishi, T. 1984 The forces and couples acting on two nearly touching spheres in low-Reynolds number flow. *Z. Angew. Math. Phys.* **35**, 634–641.

Kim, S. & Karrila, S. J. 1991 *Microhydrodynamics: Principles and Selected Applications*. Butterworth–Heinemann.

Ladyzhenskaya, O. A. 1969 *The Mathematical Theory of Viscous Incompressible Flow*. Gordon and Breach.

Leighton, D. & Acrivos, A. 1987*a* Measurement of shear-induced self-diffusion in concentrated suspensions of spheres. *J. Fluid Mech.* **177**, 109–131.

Leighton, D. & Acrivos, A. 1987*b* The shear-induced migration of particles in concentrated suspensions. *J. Fluid Mech.* **181**, 415–439.

Mammoli, A. A. 2002 Towards a reliable method for predicting the rheological properties of multiphase fluids. *Engng Anal. Bound. Elem.* **26**, 747–756.

Mammoli, A. A. 2005 The treatment of lubrication forces in boundary integral equations. *Proc. R. Soc. Lond.* A **462**, 855–881.

Mammoli, A. A. & Ingber, M. S. 2000 Parallel multipole BEM simulation of two-dimensional suspension flows. *Engng Anal. Bound. Elem.* **24**, 65–73.

Marchioro, M. & Acrivos, A. 2001 Shear-induced particle diffusivities from numerical simulation. *J. Fluid Mech.* **443**, 101–128.

Morris, J. F. & Boulay, F. 1999 Curvilinear flows of noncolloidal suspensions: The role of normal stresses. *J. Rheol.* **43**, 1213.

Nasseri, S., Phan-Thien, N. & Fan, X. J. 2000 Lubrication approximation in completed double layer boundary element method. *Comput. Mech.* **26**, 388–397.

Nott, P. & Brady, J. F. 1994 Pressure-driven flow of suspensions: Principles and computational methods. *J. Fluid Mech.* **275**, 157–199.

O'Neill, M. E. & Majumdar, S. R. 1970*a* Asymmetrical slow viscous fluid motion caused by the translation or rotation of two spheres. Part II. asymptotic forms of the solutions when the minimum clearance between the spheres approaches zero. *Z. Angew. Math. Phys.* **21**, 180–187.

O'Neill, M. E. & Majumdar, S. R. 1970*b* Asymmetrical slow viscous fluid motions caused by the translation or rotation of two spheres. Part I. The determination of exact solutions for any values of the ratio of radii and separation parameters. *Z. Angew. Math. Phys.* **21**, 164–179.

Phillips, R. J., Armstrong, R. C., Brown, R. A., Graham, A. L. & Abbott, J. R. 1992 A constitutive equation for concentrated suspension that accounts for shear-induced particle migration. *Phys. Fluids* A **4**, 30–40.

Pozarnik, M. & Skerget, L. 2003 Boundary element method numerical model based on mixture theory of two-phase flow. In *Computational Methods in Multiphase Flow II* (ed. A. A. Mammoli & C. A. Brebbia), pp. 3–12. WIT Press.

Rampall, I., Smart, J. R. & Leighton, D. T. 1997 The influence of surface roughness on the particle-pair distribution function of dilute suspensions of non-colloidal spheres in simple shear flow. *J. Fluid Mech.* **339**, 1–24.

Sangani, A. S. & Mo, G. 1994 Inclusion of lubrication forces in dynamic simulations. *Phys. Fluids* **6**, 1653–1662.

Sangani, S. & Mo, G. 1996 An $O(n)$ algorithm for Stokes and Laplace interactions of particles. *Phys. Fluids* **8**, 1990–2010.

Sierou, A. & Brady, J. F. 2001 Accelerated Stokesian dynamics simulations. *J. Fluid Mech.* **448**, 115–146.

Sierou, A. & Brady, J. F. 2002 Rheology and microstructure in concentrated noncolloidal suspensions. *J. Rheol.* **46**, 1031–1056.

Telles, J. C. F. & Oliveira, R. F. 1994 Third degree polynomial transformation for for boundary element integrals: Further improvements. *Engng Anal. Bound. Elem.* **13**, 135–142.

Tetlow, N., Graham, A. L., Ingber, M. S., Subia, S. R., Mondy, A. L. & Altobelli, S. A. 1998 Particle migration in a Couette apparatus: Experiment and modeling. *J. Rheol.* **42**, 307–327.

Youngren, G. K. & Acrivos, A. 1973 Stokes flow past a particle of arbitrary shape: A numerical method of solution. *J. Fluid Mech.* **60**, 377–403.

Zinchenko, A. Z. 1998 Effective conductivity of loaded granular materials by numerical simulation. *Phil. Trans. R. Soc. Lond.* A **356**, 2953–2998.

https://doi.org/10.1017/S0022112007000043 Published online by Cambridge University Press